



Performance-based design and manufacturing of filament wound Type-4 cylinders for compressed gas storage

Pranjali Sharma, Swati Neogi*

Indian Institute of Technology Kharagpur, India



ARTICLE INFO

Keywords:

Composite thickness distribution
Raw material consumption
Burst pressure and weight using FEA
Experimental validation

ABSTRACT

Filament wound type-4 cylinders are widely used in automotive applications for the storage of compressed gases. The performance of the storage cylinders critically depends on their manufacturing parameters. These parameters include the material properties of the reinforcement and matrix material, the number of fiber spools used during winding, the fiber bandwidth, the initial fiber band volume fraction, the mandrel geometry, the winding sequence, and the composite layer thickness distribution. An interim link between the critical parameters, the composite thickness distribution and the amount of fiber and resin consumed for winding a type-4 composite vessel has been established using an analytical model in this study. The developed model is validated by manufacturing the cylinder and comparing the theoretical and experimental results. The composite layer distribution across the entire geometry of the vessel is included into an FEA model to predict the burst pressure and weight of the obtained type-4 cylinder with greater precision. The given study can be used to design low-cost high burst performing type-4 composite structures with significant weight reduction.

1. Introduction

The filament winding process is a widely adopted manufacturing technique for fabricating type-4 composite cylinders for compressed gas storage [1–4]. The composite overwrap functions as the backbone of the storage system, providing strength for pressurized gas storage[5]. The composite thickness distribution, mandrel geometry, winding pattern, winding angle, and manufacturing technique affect the load-bearing characteristics of the reinforcing fibers supported by proper load transfer in the resin medium [6–10]. Unidirectional fiber reinforced composites are orthotropic materials that mainly bear loads in longitudinal directions[11–13]. The winding angles, sequence of layers, and individual layer thicknesses at different dome locations are arranged to target proper structural strength in all directions[14–16]. The winding angles and the layer sequence are predetermined based on design pressure and estimated layer thicknesses[17–20]. The pressure vessel is designed to bear required load and a variety of literature emphasizes on different aspects of vessel design. The orientation of fibers and their location in the composite strongly allows to shape its strength for a given set of possible loads[21–23]. While, the failure of the vessel depends on the material properties, the vessel design, manufacturing, and loading conditions[24]. However, the composite thickness while doing actual

winding varies with fiber bandwidth, fiber winding path, liner geometry, and the initial fiber volume fraction [25–29]. Fu et al. have generated geodesic or nongeodesic trajectories for filament winding based on the StereoLithography model to predict the winding trajectories[30]. For a type-4 composite vessel, the liner acts as the mandrel for the winding process without contributing much to the total strength of the composite cylinder[27,31]. Many works on enhancing the individual properties of the composites, stress and failure analysis of composite laminates, winding angle optimization using FEA, etc. have been reported in the literature.

Magnucki et al. designed and analyzed a better-performing dome head for a cylindrical pressure vessel[32]. Li et al. identified the failure criterion for predicting material failure, instability, buckling, crippling, and delamination of filament wound type-4 composite cylinders[33]. Kobayashi et al. investigated the effects of stacking thickness on the microscopic damage behavior in type-4 composite cylinders subjected to quasi-static loading[34]. Liu et al. presented a review article on the optimization of composite design for predicting burst pressure and fatigue life[35]. Leh et al. optimized the composite stacking sequence type-4 cylinders[36]. Colombo et al. designed a model for the selection of the optimal fiber, matrix, volume fraction, and winding angle θ for winding composite pipes[37]. Structural failure of the pipe subjected to

* Corresponding author.

E-mail address: swati@che.iitkgp.ac.in (S. Neogi).

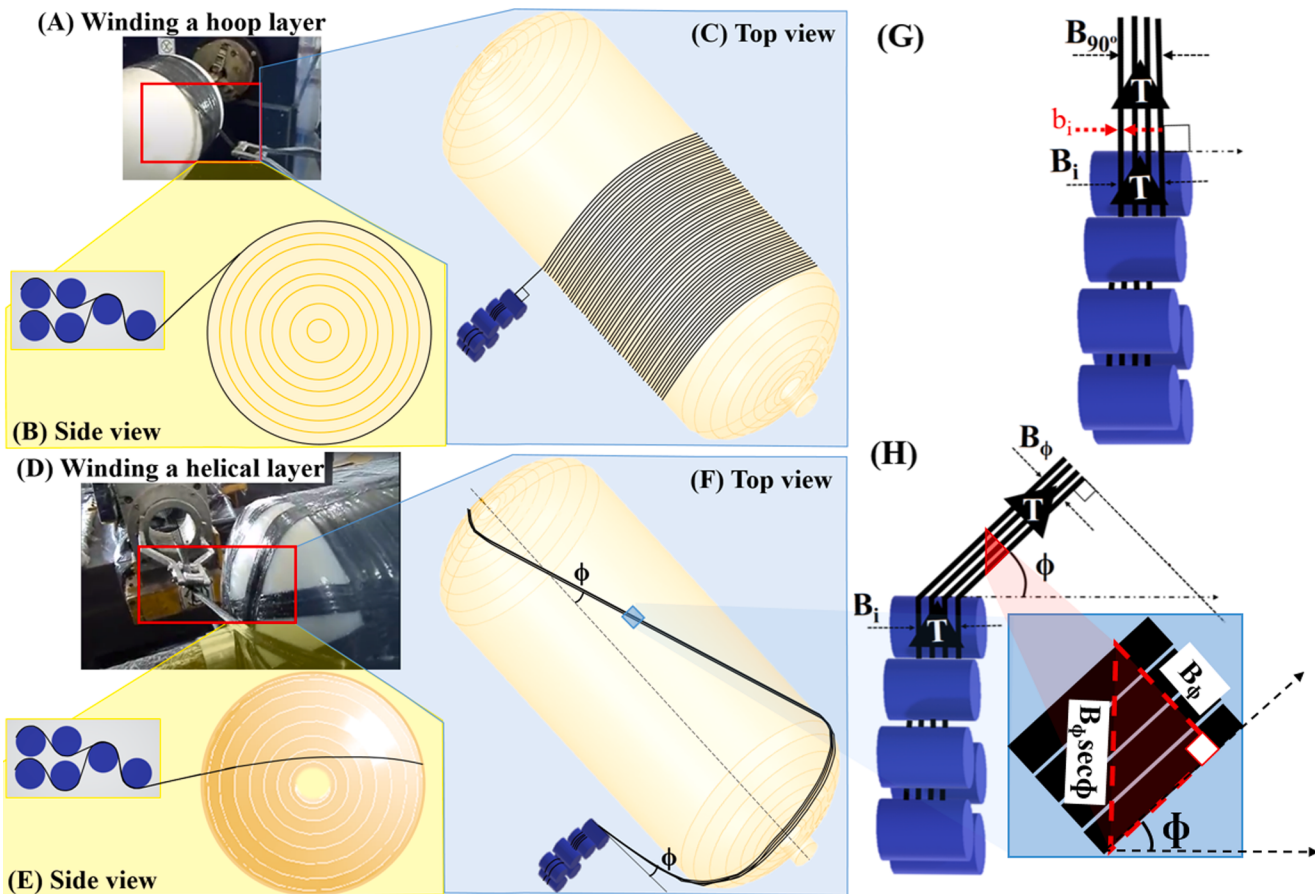


Fig. 1. (A) Winding, (B) side view, (C) top view of hoop layer, (D) winding, (E) side view, (F) top view of helical layer, magnified delivery eye for (G) hoop, and (H) helical winding.

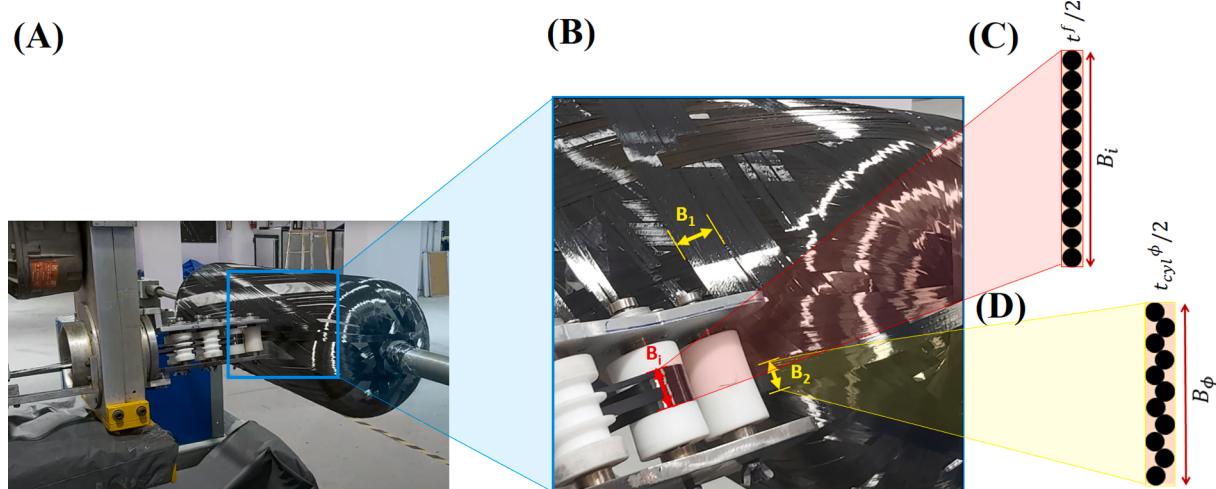


Fig. 2. (A) Winding composite layers, (B) magnified view of bandwidths for different winding angles, schematic for (C) initial bandwidth, and (D) non-hoop angle bandwidth.

transverse loading has also been reported [38–40]. A 3-axis filament winding machine was also designed and optimized [41].

However, no one as per our knowledge has derived and experimentally validated an analytical model to determine the individual/total thickness distribution of filament wound type-4 composite structures. Hence, an analytical model is developed to predict the composite thickness distribution of the filament wound type-4 vessel along with the total raw material consumption. The effects of fiber bandwidth, fiber

band volume fraction, and winding pattern on the composite thickness distribution of the composite are analyzed. The predicted composite thickness distribution is compared with the cross-section of a dissected filament wound type-4 composite cylinder. An FEA model is developed to determine the burst pressure, failure characteristics, and weight of the type-4 vessel with the composite thickness distribution obtained using the analytical model. The FEA model is validated by manufacturing the designed cylinder, weighing the cylinder, and testing it for the

Table 1

Bandwidth, thickness, and winding cycle calculations for different winding angles.

Winding angle (°)	Bandwidth at opening radius (mm)	Thickness at opening radius (mm)	Thickness in cylindrical section (mm)	Bandwidth in cylindrical section (mm)	Number of cycles to wind a layer
7.5	2.763	4.528	0.688	18.185	117
15	5.624	2.225	0.639	19.579	106
25	9.7868	1.278	0.626	19.986	97
35	14.695	0.851	0.613	20.410	86
45	20.983	0.596	0.601	20.817	73
90	21	0.596	0.596	21	70

hydrostatic pressure burst test. The validated FEA model is used for optimizing the fiber bandwidth, the initial fiber band volume fraction, and the winding pattern for better burst and weight performance. Composite thickness distribution that yields higher burst pressure with the least system weight is obtained. The raw material cost for manufacturing a cylinder with optimized composite layer distribution is also estimated for glass, Kevlar, and carbon fiber reinforcement materials.

2. Theory and calculations

The filament winding process is modeled to predict the composite thickness and bandwidth at any location on the mandrel. The results of this analytical model can be used to predict the exact fiber thickness distribution after fiber bundling at the dome section. It can also be used to estimate the layer-wise fiber consumption for calculating the approximate weight of the type-4 cylinder and the raw material cost. The results of this analytical model are used to predict the burst pressure and failure characteristics of the type-4 vessel with greater precision using FEA.

2.1. Determination of bandwidth and band-thickness

Bandwidth is the overall width of the fiber band being delivered from the payout eye to the mandrel surface. The cylinders are wound using one to six fiber spools simultaneously. The filament bundles from each spool are arranged side by side at the payout eye using a proper pulley placement system. The bandwidth at which the filament bundles are laid at the delivery eye is known as the initial bandwidth (B_i) as seen in Fig. 1 (G) and 1(H). It depends on the bandwidth of individual fiber spools, the percentage overlap between the adjacent fiber bands, and the number of fiber spools constituting the total fiber bandwidth at the payout eye, as given in Equation (1). The bandwidth changes significantly when a helical layer is wound; the fiber path trajectories for hoop and helical winding are compared in Fig. 1(C) and 1(F). The movement of the payout eye is also compared in Fig. 1(A), 1(B), 1(D), and 1(E). The fiber path for helical winding is deviated by an angle equivalent to the winding angle at the delivery eye as seen in Fig. 1(H).

Composite layers wound at smaller winding angles have overlapped fiber bands near the opening radius of the fiber winding path. The band-thickness increase and the bandwidth decrease as shown in Fig. 2(D). Only hoop layers with 90° winding angles are wound with initial bandwidth as in Fig. 2(C); the hoop layer thickness is the least for the entire winding process. The payout eye inclines the fiber bands at the required winding angles as seen in Fig. 2(A) and 2(B). The decrease in bandwidth is due to this inclined tensioning at the opening radius of the fiber winding path, as shown in Fig. 1(H). The initial bandwidth at the delivery eye and the bandwidth obtained on the mandrel surface are correlated by assuming uniform tension across the fiber band spread as given in Equation (1) for helical layer winding.

$$B_i = N_i * O\% * b_i; B_{\phi} = B_i \tan \phi \quad (1)$$

Where ϕ is the winding angle, B_i is the initial bandwidth at the delivery eye, b_i is the bandwidth of a single fiber spool i.e. 3.5 mm for this case, N_i is the number of fiber spools that constitute a fiber band for winding i.e. 6 in this case, O% is the fraction of reduction in bandwidth of individual fiber bands due to overlapping at the payout eye, $B_{\phi,0}$ is the bandwidth of the helical layer at the opening radius of the fiber path.

The initial fiber volume fraction is estimated using the mass and density of individual fibers and the resin being wound on the mandrel surface per minute. Fibers are assumed to be cylinders whose length depends on the winding speed and mass depends on the linear density. The initial fiber volume fraction is calculated using the material properties of the fiber, the winding speed, and the amount of resin consumed per minute during winding as given in Equation (2).

$$V_{f0} = \frac{N_i * \rho_r * tex_f * W_i}{N_i * \rho_r * tex_f * W_i + 10^6 * \rho_f * M_r} \quad (2)$$

Where V_{f0} is the initial fiber volume fraction in fiber bands at the payout eye, tex is the linear density of the fiber i.e. 800gm/1000 m for T700SC-12 k carbon fiber, M_r is the net mass of resin consumed from the resin drum per minute, W_i is the winding speed for rotating the mandrel in mm/min, ρ_f and ρ_r are the densities of the fiber and the resin components respectively.

The cross-sectional area of the resin dipped fiber bands at any position on the mandrel surface and the pay-out eye will remain constant based on principles of volume conservation. It is represented as given in Equation (3) and illustrated in Fig. 2.

$$B_i * t_{hoop} = B_{\phi} * t_{\phi} = \frac{2 * N_i * tow * \pi R_f^2}{V_{f0}} \quad (3)$$

Where the bandwidth for winding hoop layers is equivalent to the initial bandwidth as no path deviation is observed for hoop winding. B_{ϕ} is the bandwidth of the helical layer with winding angle ϕ , t_{ϕ} is the thickness of that layer at the same location, R_f is the fiber radius which is 3.5 μm for T700SC-12 k carbon fiber, tow is the number of filaments constituting a carbon fiber which is 12000, and t_{hoop} is the thickness of the hoop layer.

The surface area covered by the composite layers in the dome section reduces as the dome radius is tapered towards the ends. Therefore, the thickness at those locations increases based on the principle of volume conservation. The product of thickness and surface area of the cylinder at given axial location remains constant as filament winding is an axisymmetric process. The layer thickness is highest at the opening radius of the fiber winding path due to the bundling of fiber bands. For a helical layer, Equation (4) is used to establish a relation between the layer thickness at the cylindrical section and that at different dome locations [15].

$$t_{dome} = t_{cylinder} \left(\sqrt{\frac{R_{cylinder}^2 - (R_{opening})^2}{R_{location}^2 - (R_{opening})^2}} \right) \quad (4)$$

Where t_{dome} is the layer thickness at a given dome position, $t_{cylinder}$ is the layer thickness in the cylindrical region, $R_{cylinder}$ is the equator radius of the dome, and $R_{opening}$ is the opening radius for the fiber winding path.

The number of cycles completed by the payout eye for winding a hoop or helical layer is calculated using Equation (5). One cycle signifies the movement of the delivery eye from one end of the mandrel to another and back to the previous end. While winding a helical layer signifies winding the mandrel with $+\phi$ winding angles in one cycle followed by $-\phi$ in another cycle, hereby completing the winding of $\pm\phi$ winding angle. The hoop layers aim to cover the cylindrical length completely, while the helical layers cover the circumference of the pressure vessel in the cylindrical section without leaving gaps in between adjacent fiber bands.

Table 2

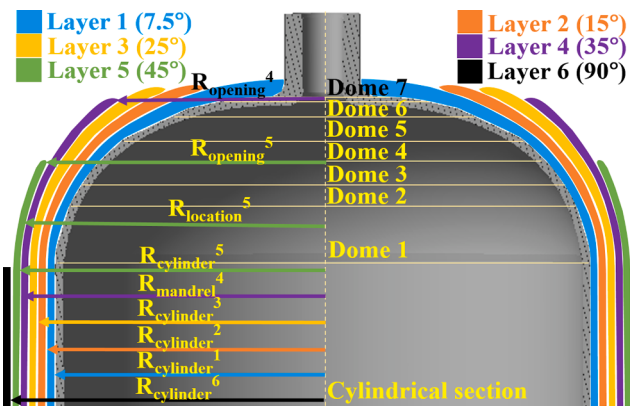
Layer thickness at a given radial location on the plastic liner surface.

Angle (°)	Layer thickness at given radial location (mm)							
	Cylinder	Dome 1	Dome 2	Dome 3	Dome 4	Dome 5	Dome 6	Dome 7
7.5	0.688	0.696	0.734	0.803	0.929	1.408	2.089	3.513
15	0.639	0.647	0.684	0.753	0.88	1.413	2.432	0
25	0.626	0.716	0.749	0.813	0.941	1.006	0	0
35	0.613	0.626	0.658	0	0	0	0	0
45	0.601	0.648	0	0	0	0	0	0
90	0.596	0	0	0	0	0	0	0

Table 3

Winding pattern of the type-4 composite overwrap.

Winding angles	Number of layers	Layer thickness
90°, 45°, 35°, 25°, 15°, 7.5°	29	~17 mm

**Fig. 3.** Significance of different radial locations for layer thickness calculations.

$$n_{i,\phi} = \frac{4\pi R_{mandrel}}{B_{\phi,cyl} \sec \phi}; n_{i,90} = \frac{2L_{mandrel}}{B_i} \quad (5)$$

Where $B_{\phi,cyl}$ is the bandwidth of helical layer in cylindrical section, and $R_{location}$ is the radius of the location at which thickness is determined. n_i is the number of winding cycles the payout eye completes to wind one composite layer and $L_{mandrel}$ is the length of the cylindrical section of the mandrel.

For an initial fiber bandwidth of 21 mm and an initial fiber volume fraction of 0.39 ± 0.02 , the hoop layer thickness for $\pm 90^\circ$ winding using Equations (1) to (4) is calculated to be 0.596 mm. Similarly, the fiber bandwidths at the opening radius and cylindrical regions, layer thicknesses and different locations, and the number of cycles required for winding one layer are calculated and summarized in Table 1 below. These values are calculated for winding the first layer, where the liner

surface acts as the mandrel geometry.

The layer thickness distribution in the dome section depends on the initial fiber volume fraction of the fiber bands, the diameter of the mandrel, the opening radius of the fiber winding path, and the radial location of the section for which the layer thickness has to be determined. The layer thicknesses at different locations to wrap a composite layer with a given winding angle over the liner surface are calculated using Equations (1) to (5) and are summarized in Table 2.

2.2. Individual and overall thickness distribution for a given winding pattern.

A winding sequence of the cylinder is obtained based on the results of winding trials for ease of winding. The details of the obtained winding pattern are given in Table 3 below. The approximate composite thickness of the vessel in the cylindrical section as per the results of Table 1 is estimated to be ~ 17 mm. However, the actual thickness distribution may vary as these values are calculated for winding first layers where the mandrel geometry follows the liner dimensions.

As the winding progress, the composite thickness of previously wound layers is added to the geometry of the mandrel to act as the new mandrel for winding the consecutive composite layers. The geometry changes significantly in the dome section due to fiber bundling effects. Therefore, for estimating the thicknesses of the later layers precisely, the model is extended for including these changes in mandrel geometry. The mandrel dimensions for calculations of the individual thickness of the composite layers wound over pre-existing composite layers are calculated using Equation (6) as illustrated in Fig. 3.

$$R_{i+1} = R_i + t_i \quad (6)$$

R_{i+1} is the radius of the mandrel for winding $i + 1$ th composite layer at that location, R_i is the radius of the mandrel of the previously wound layer at a particular radial location, and t_i is the corresponding calculated thickness for i^{th} layer at that location.

The layer thickness for winding a layer over previously wound layers is calculated using Equation (7).

$$t_{location,m} = \frac{2 * N_i * tow * \pi R_f^2}{V_{f,0} * B_i * \tan \phi} \left(\sqrt{\frac{(R_{opening} + B_{\phi,cyl} + \sum_{i=1}^{m-1} t_{opening,i})^2 - (R_{opening} + \sum_{i=1}^{m-1} t_{opening,i})^2}{(R_{location} + \sum_{i=1}^{m-1} t_{location,i})^2 - (R_{opening} + \sum_{i=1}^{m-1} t_{opening,i})^2}} \right) \quad (7)$$

Table 4

Composite layer thicknesses at different sections of the type-4 cylinder.

Cylinder (mm)	Dome 1 (mm)	Dome 2 (mm)	Dome 3 (mm)	Dome 4 (mm)	Dome 5 (mm)	Dome 6 (mm)	Dome 7 (mm)
16.61	10.95	11.19	11.75	13.61	18.5	28.32	37.59

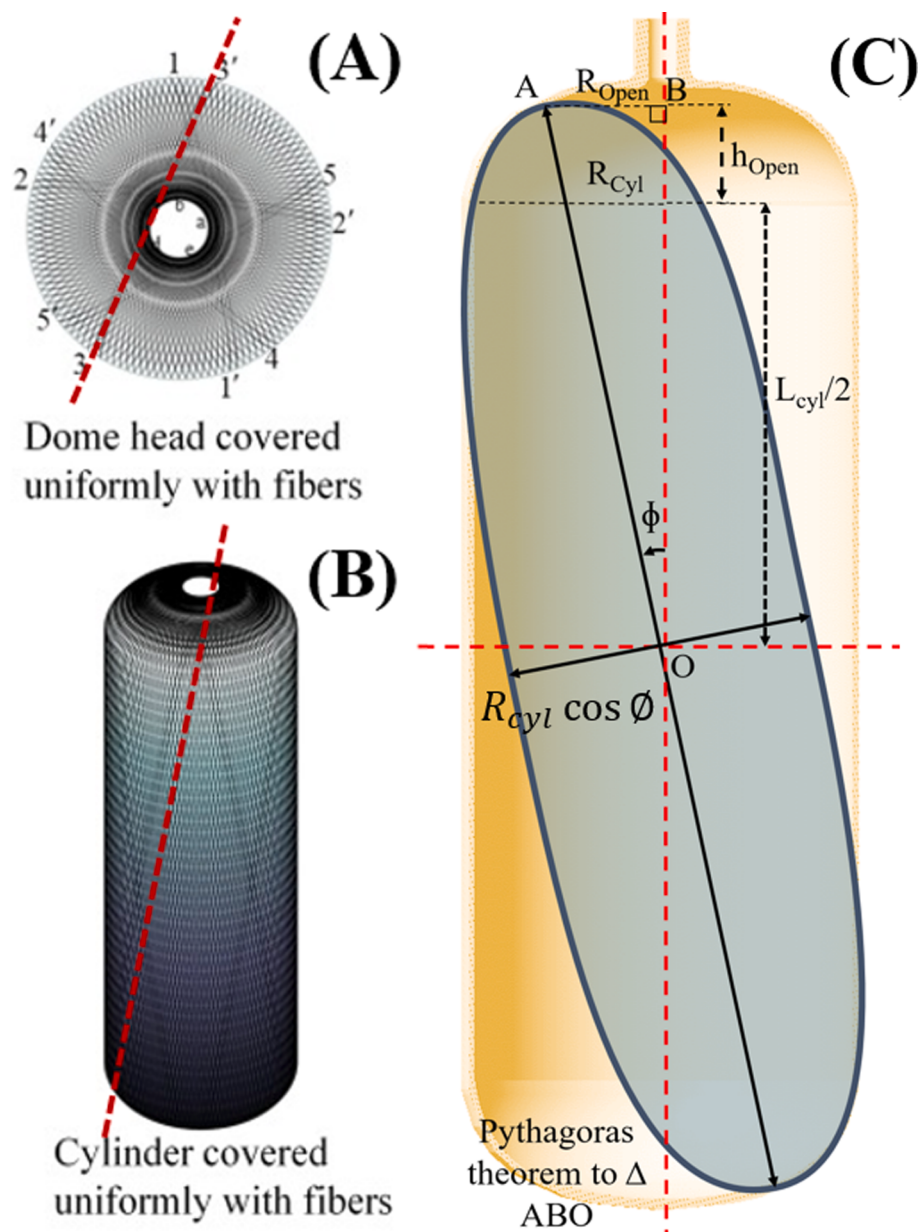


Fig. 4. (A) Top view, (B) front view of fiber trajectory, and (C) projected ellipse for winding a helical layer.

Where $t_{\text{location},m}$ is the composite layer thickness of the m^{th} winding layer at a given radial location, $t_{\text{opening},i}$ is the thickness of i^{th} winding layer at the opening radius of the fiber winding path, and $t_{\text{location},i}$ is the composite layer thickness of the i^{th} winding layer at the same radial location for which the thickness for m^{th} layer is to be determined. The remaining parameters have been defined in the description of Equations (1) to (5). The results are summarized in Table 4. The order in which the dome section is distributed is illustrated in Fig. 3.

2.3. Layer wise fiber consumption

The mass of the fibers used to wind a given hoop or helical layer is calculated assuming that the fiber trajectory for winding cycles are ellipsoidal. The consumption of fibers depends on the length of fiber required to cover one cycle, the total number of cycles required to wind layer as calculated using Equations (4) and (5), and the linear density of the fibers. The circumference of the cylindrical section of the mandrel is the length of the fiber consumed in one hoop winding cycle. During

helical winding, the fiber length is the perimeter of the projected area which follows the fiber path as shown in Fig. 4(C); the perimeter of an ellipse is calculated using Equation (8).

$$\text{Perimeter}_{\phi \text{ ellipse}}^i = 2\pi \sqrt{\frac{a^2 + b^2}{2}} \quad (8)$$

Where a and b are the major and minor axis of the ellipse. In the case of polar winding, the entire path is an ellipse, while helical layers with higher winding angles comprise 2–3 ellipses. This value depends on the angle which is wound and the length of the cylindrical section of the mandrel. Equations (9) and (10) are used for calculating the mass of fiber consumed for winding hoop and helical layers respectively.

$$m_{\text{hoop}}^i = \frac{4\pi R_{\text{mandrel}} * N_i * L_{\text{cyl}} * \text{tex}}{B_i} \quad (9)$$

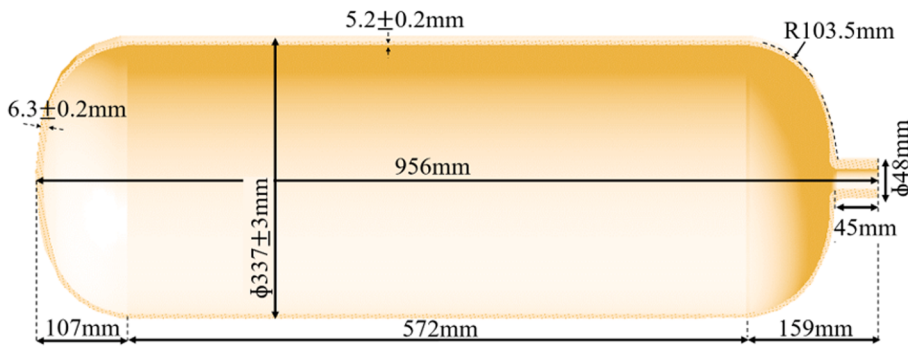


Fig. 5. Geometry of the plastic liner.

Table 5
Elastic properties of T700SC-12 k carbon fiber and Araldite resin/hardener system.

Property	Symbol and unit	Value for fiber	Value for resin
Longitudinal modulus	E_{11} (MPa)	230,000	3450
Transverse modulus	E_{22} (MPa)	17,000	3450
Inplane shear modulus	G_{12} (MPa)	9000	1280
Shear modulus in YZ plane	G_{23} (MPa)	4600	1280
Major Poisson's ratio	ν_{12}	0.2	0.35
Poisson's ratio	ν_{23}	0.25	0.35
Longitudinal tensile strength	X_{11}^f (MPa)	4900	90
Longitudinal compressive strength	X_{11}^c (MPa)	2500	130
Shear strength	X_{12} (MPa)	600	50
Stress in matrix at fiber break	s_{11}^f (MPa)	NA	0.148

$$m_{\phi}^i = \frac{4\sqrt{2}\pi^2 * N_i * tex * R_{mandrel}}{B_{\phi,cyl_i} \sec\phi_i} \sqrt{R_{open_i}^2 + (R_{mandrel} \cos\theta_s)^2 + \left(h_{open_i} + \frac{l_{cyl}}{2}\right)^2} \quad (10)$$

Where h_{open} is the height of the dome curvature at R_{open} as the radial location. The remaining notations are the same as those used in Equations (1) to (5).

The limitations of the developed analytical model include the requirement of initial winding trials to determine the exact values of opening radii for no-slippage during winding. The fiber winding path is assumed to be ellipsoid for estimation of the fiber length, however the actual path is slightly deviated from the projected ellipsoid trajectory. This assumption doesn't affect the calculations significantly as seen while validating the model using experimental results.

2.4. Failure theories for the FEA model

The burst pressure, failure characteristics, and weight of the vessel are calculated using the finite element method. The thickness distribution results of the analytical model are incorporated into the FEA model to accurately predict burst failure and the weight of the filament wound type-4 cylinder. The type-4 composite vessel with the calculated thickness distribution is constructed using FEA and analyzed for its response to applied internal pressure in form of compressed gas. Maximum stress, maximum distortion, Tsai-Wu, Tsai-Hill, Hoffman, and Hashin failure criteria are used to predict failure. The internal load conditions are changed for which the normal and shear stress components are recorded. For predicting layer-wise failure, the composite elements are independently defined for layered shell elements. The stress components generated in discrete composite layers are determined to predict the failure in solution coordinate system. For a given layer, the values of stress components along -X, -Y, and -Z directions are determined for failure analysis; the stress values along -Z directions are obtained to be

tending to zero in the chosen coordinate plane. Few failure theories evaluate failure in plane strain mode i.e., they assume normal stress components along the z-direction and shear stress components in YZ- and XZ-planes to be zero. While the other failure criteria consider the -Z components for failure evaluation. The composite elements being defined in the solution coordinate system has stress values mainly defined in -X and -Y directions and -Z components tend to zero, inherently satisfying the requirements of all the failure criteria.

The internal loads for which the failure parameters as given in Equations (11) to (16) have a value of equal to or greater than one are taken as failed zones of the cylinder as per that failure theory [42]. The failure parameter ξ_0 as defined in Equation (11) corresponds to failure as per maximum principle stress criterion. Similarly, failure parameters ξ_1 , ξ_2 , ξ_3 , ξ_4 , and ξ_5 corresponds to failure as per maximum distortion, Tsai-Wu, Tsai-Hill, Hoffman, and Hashin failure criteria in Equations (12) to (16) respectively.

$$\xi_0 = \frac{\sigma_x}{\sigma_{xf}} \text{ or } \frac{\sigma_x}{\sigma_{xcf}} \text{ or } \frac{\sigma_y}{\sigma_{yf}} \text{ or } \frac{\sigma_y}{\sigma_{ycf}} \text{ or } \frac{\sigma_{xy}}{\sigma_{xyf}} \quad (11)$$

$$\xi_1 = \frac{\sigma_{eq}}{\sigma_{xf}} \quad (12)$$

$$\xi_2 = \frac{1}{\frac{-E}{2S} + \sqrt{\left(\frac{E}{2S}\right)^2 + \frac{1}{S}}} \quad (13)$$

$$\text{Where, } S = \frac{-\sigma_x^2}{\sigma_{xf}\sigma_{xcf}} - \frac{\sigma_y^2}{\sigma_{yf}\sigma_{ycf}} + \frac{\sigma_{xy}^2}{(\sigma_{xy})^2} + \frac{C_{xy}\sigma_x\sigma_y}{\sqrt{\sigma_{xf}\sigma_{xcf}\sigma_{yf}\sigma_{ycf}}} \quad (14)$$

$$F = \left(\frac{1}{\sigma_{xf}} + \frac{1}{\sigma_{xcf}} \right) \sigma_x + \left(\frac{1}{\sigma_{yf}} + \frac{1}{\sigma_{ycf}} \right) \sigma_y$$

Where C_{xy} , C_{yz} , and C_{xz} are Tsai Wu coupling coefficients.

$$\xi_3 = \frac{\sigma_x^2}{(\sigma_{xf})^2} + \frac{\sigma_y^2}{(\sigma_{yf})^2} - \left(\frac{1}{(\sigma_{xf})^2} + \frac{1}{(\sigma_{yf})^2} - \frac{1}{(\sigma_{zf})^2} \right) \sigma_x \sigma_y + \frac{\sigma_{xy}^2}{(\sigma_{xy})^2} \quad (15)$$

$$\xi_4 = \frac{\sigma_x^2}{\sigma_{xf}\sigma_{xcf}} + \frac{\sigma_y^2}{\sigma_{yf}\sigma_{ycf}} + \frac{\sigma_{xy}^2}{(\sigma_{xy})^2} - \frac{\sigma_x\sigma_y}{\sigma_{xf}\sigma_{xcf}} + \left(\frac{1}{\sigma_{xf}} - \frac{1}{\sigma_{xcf}} \right) \sigma_x + \left(\frac{1}{\sigma_{yf}} - \frac{1}{\sigma_{ycf}} \right) \sigma_y \quad (16)$$

Tensile and compressive fiber failures and matrix failure under tension are defined using Equation (16).

$$\xi_{fiberfailure} = \frac{\sigma_x^2}{(\sigma_{xf})^2} + k.\alpha \frac{\sigma_{xy}^2}{(\sigma_{xy})^2}; \xi_{matrixfailure} = \frac{\sigma_y^2}{(\sigma_{yf})^2} + \frac{\sigma_{xy}^2}{(\sigma_{xy})^2} \quad (17)$$

Where α is the Hashin coefficient in the range of 0 to 1, k is the load factor whose value is unity for tensile loads and null for compressive loads.

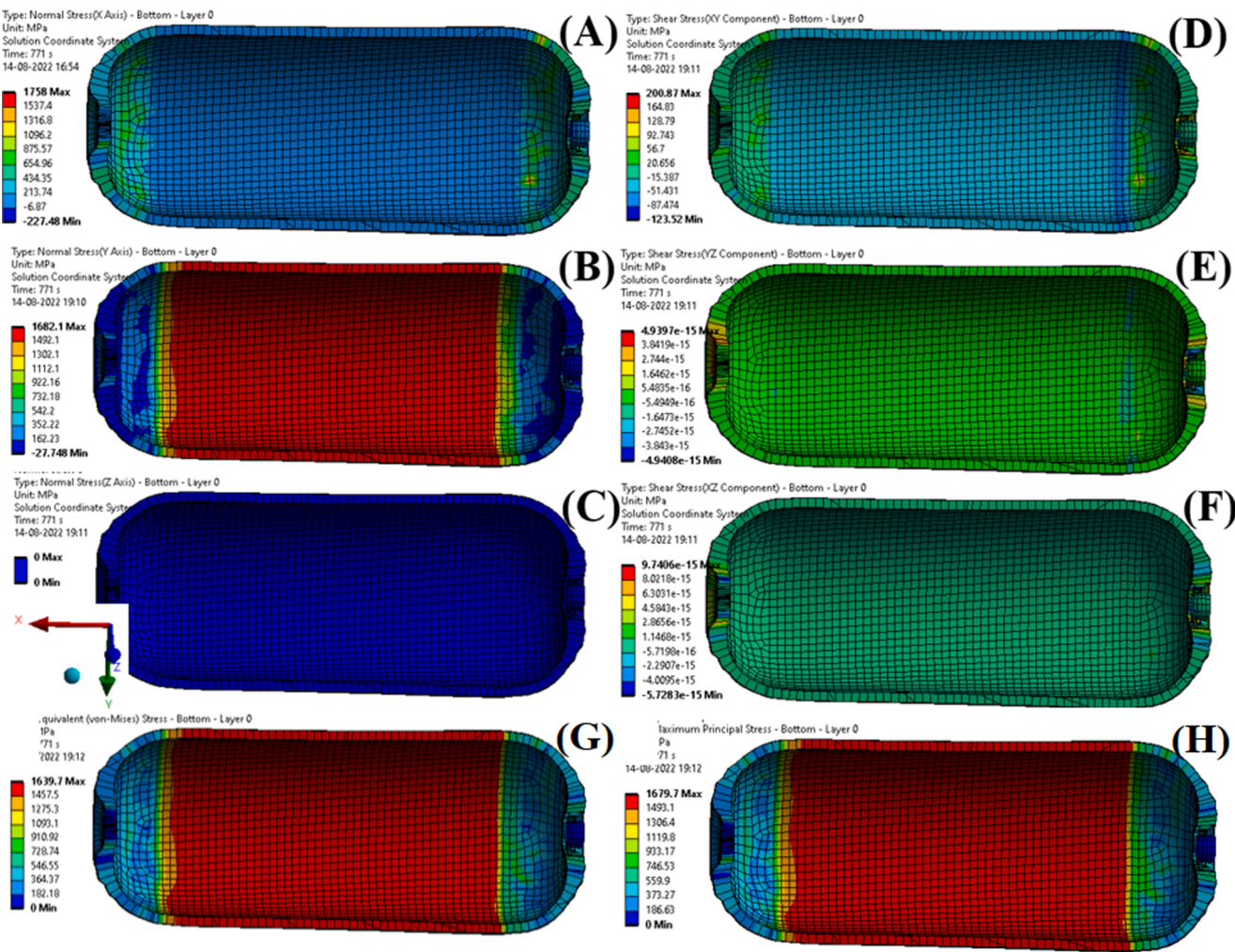


Fig. 6. Normal stress along (A) X-, (B) Y-, (C) Z- axis, and shear stress in (D) XY-, (E) YZ-, (F) XZ- plane, (G) equivalent, and (H) maximum principle.

Table 6

Manufacturing parameters used for winding the type-4 composite cylinder.

Location	Tension	Initial bandwidth	Winding speed
Cylinder	5.2–9.7 N	21 mm	18000–20000 mm/min
Dome	5.2–9.7 N	Varies along dome height	2400–2500 mm/min

3. Material and methods

Akulon Fuel Lock manufactured by DSM Plastics, USA was identified as a suitable polyamide liner material for the rotomolding process. The manufactured liner acts as the base mandrel geometry for winding the first composite layer. Therefore, the fiber path for winding of initial composite layers depends on the liner geometry which is illustrated in

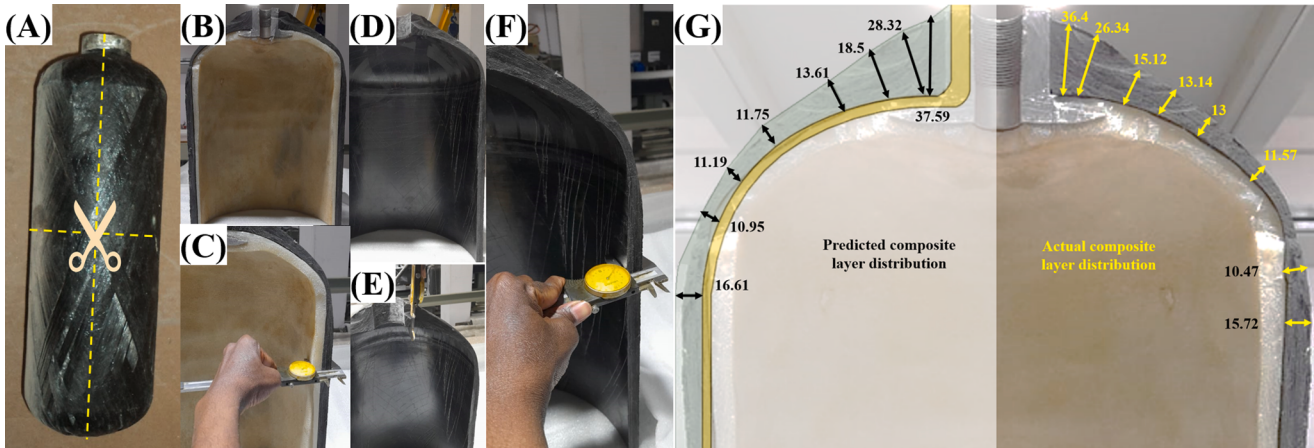


Fig. 7. (A) Dissection path, (B–C) cylinder thickness distribution (D–F) composite thickness distribution, and (G) overlap predicted with actual thickness distribution.

Table 7

Recorded information on fiber consumption during winding of prototype before and after winding a given layer and the corresponding fiber consumption from all 6 fiber spools compared with the predicted consumption per winding layer.

Layer no.	Weight of 1 CF spool (kg)		Fiber used for 6 spools (kg)	Predicted amount of fiber consumption (kg)
	Before	After		
1	3.633	3.554	0.476	0.451
2	3.554	3.407	0.882	0.857
3	3.407	3.318	0.534	0.610
4	3.318	3.236	0.492	0.456
5	3.236	3.148	0.528	0.607
6	3.148	3.052	0.576	0.549
7	3.052	2.957	0.57	0.603
8	2.957	2.876	0.486	0.462
9	2.876	2.784	0.552	0.599
10	2.784	2.7	0.504	0.565
11	2.7	2.604	0.576	0.637
12	2.604	2.526	0.468	0.468
13	2.526	2.428	0.588	0.692
14	2.428	2.345	0.498	0.471
15	2.345	2.246	0.594	0.588
16	2.246	1.939	1.842	1.129
17	1.939	1.892	0.282	0.327
18	1.892	1.73	0.972	0.978
19	1.73	1.603	0.762	0.822
20	1.603	1.552	0.306	0.420
21	1.552	1.309	1.458	1.283
22	1.309	1.236	0.438	0.416
23	1.236	1.165	0.426	0.513
24	1.165	1.058	0.642	0.588
25	1.058	0.957	0.606	0.600
26	0.957	0.865	0.552	0.490
27	0.865	0.754	0.666	0.524
28	0.754	0.678	0.456	0.494
29	3.6	3.554	0.42	0.526
Total Fiber consumption	18.152 kg		17.827 kg	
Total Resin consumption	12.50 kg		12.28 kg	

Fig. 5 below.

T700SC-12000 carbon fiber from Toray, Japan is used as the reinforcement material. Araldite LY556 and Hardener XY-54 are the matrix components manufactured by Huntsman, USA. The obtained value of fiber volume fraction is 0.4 ± 0.01 , as given in Section 3.2 of this study. The fiber volume fraction and the individual properties of T700SC-12 k carbon fiber and Araldite resin as given in Table 5 are used to calculate the elastic properties of the composite using the micromechanics

approach.

3.1. Developing an FEA model

The burst pressure, failure characteristics, and weight of the type-4 vessel are predicted in the ANSYS workbench. The elastic properties of the composite obtained using the micromechanics approach are used as the engineering data for the FEA model. The density of the dissected composite is determined to be 1.674 g/cm^3 using an UltraPyc 1200e Automatic Gas Pycnometer, manufactured by Quantachrome Instruments. The liner geometry is defined as per the dimensional analysis of the dissected cylinder. The failure of the composite cylinder is modeled in the ACP pre-post module using SHELL181 elements. The inner curvature of the roto-molded liner is used as the geometry and layered sections over the SHELL elements constitute the exact thicknesses determined using the analytical model. CONTACT174 and TARGET170 elements act as the interface between the nylon liner and the composite plies. The inner surface of the liner is applied with an internal pressure load which increases at a ramp rate of 0.35 MPa/s using SURF154 elements. Fixed support at the open end of the liner is the applied boundary condition for the FEA model. For uniformity of analysis as explained in Section 2.4 of this study, the stress analysis is modeled in the solution coordinate system for 75 MPa of applied pressure which yields zero values of normal z-axis stress, and shear YZ- and XZ- stress components as summarized in Fig. 6. The cylinder geometry is divided into quadrilateral dominant meshes with an element size of 10 mm . The reported mesh size is the optimized value for the given geometry which gives independent results with least modelling time. Differentiating the elements further into smaller mesh elements give the same results however the time required to compute the results increase significantly for which an element size of 10 mm was preferred for the analysis.

Normal and shear stress components on individual elements are determined along with the average and maximum stress components for the entire geometry. ACP pre-post module is used to determine the failure parameter values of all the elements using different failure theories. The meshed elements whose failure parameter values as per a chosen failure criterion are greater than one are treated as the failed elements and marked by red contours in the failure characteristics as given in Figure S1 of the supplementary information. The elements on the verge of failure have a parameter value equal to one and are marked as orange, while all those with values less than one are safer regions

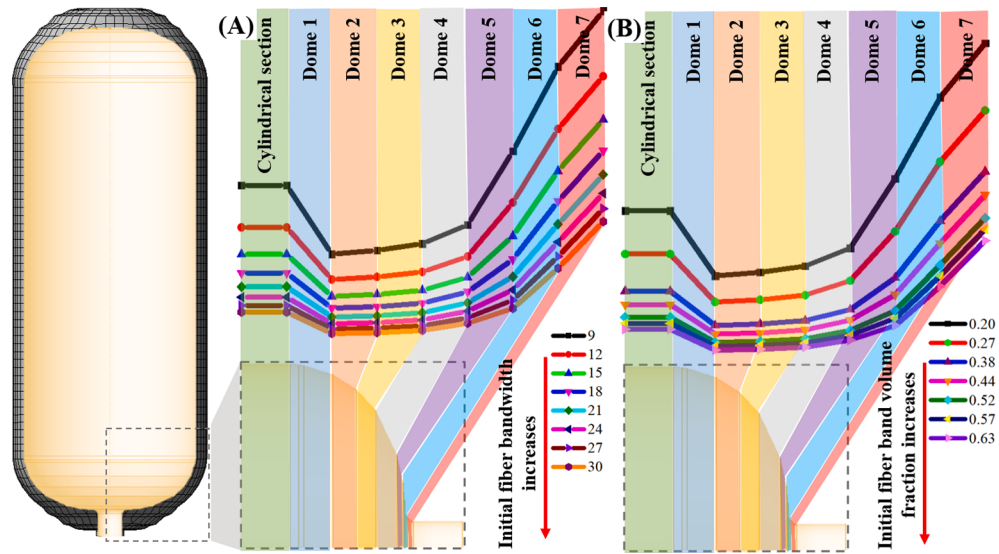


Fig. 8. Effect of (A) initial bandwidth(mm) and (B) initial fiber band volume fraction on composite thickness in different sections of the type-4 cylinder**Thickness is measured along the radial direction of the dome sections.

Table 8

Variation in composite layer thickness distribution with initial fiber volume fraction for a given winding pattern and liner geometry.

Fiber band volume fraction	Initial fiber bandwidth (mm)	Composite layer thickness distribution (mm)						
		Cylinder	Dome 1	Dome 2	Dome 3	Dome 4	Dome 5	Dome 7
0.196	21.000	34.533	22.108	22.775	23.971	27.422	40.710	56.236
0.268	21.000	26.290	17.100	17.529	18.421	21.184	30.625	43.932
0.379	21.000	19.181	12.609	12.893	13.543	15.651	21.738	32.616
0.443	21.000	16.612	10.956	11.196	11.760	13.616	18.498	28.324
0.524	21.000	14.183	9.381	9.581	10.064	11.674	15.442	24.153
0.573	21.000	13.017	8.621	8.803	9.247	10.737	13.988	22.113
0.631	21.000	11.882	7.879	8.044	8.450	9.820	12.589	20.104

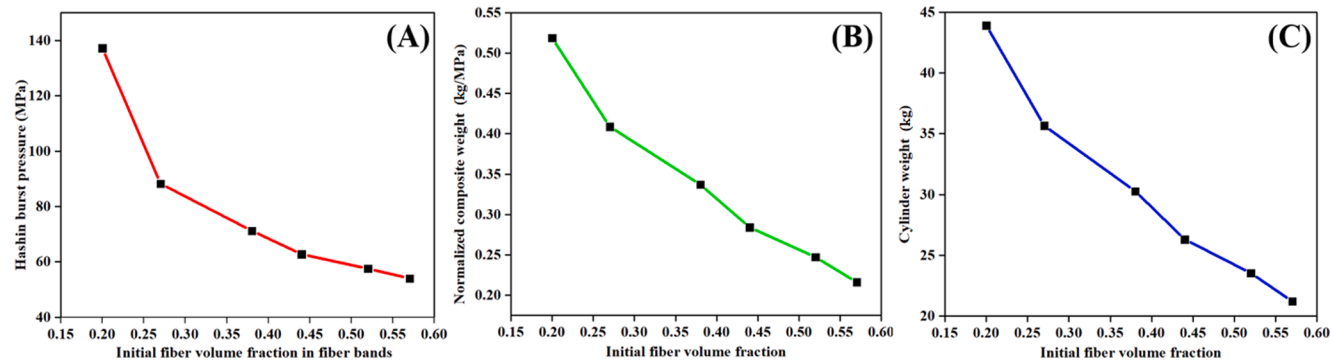


Fig. 9. Effect of initial fiber band volume fraction on (A) burst pressure, (B) normalized composite weight, and (C) cylinder weight.

Table 9

Effect of winding sequence on burst pressure and vessel weight.

Winding sequence	1	2	3
Burst pressure (MPa)	79.86 MPa	80.5 MPa	82.59 MPa
Vessel weight (Kg)	38.97 kg	37.69 kg	36.92 kg
Normalized weight (Kg/MPa)	0.488	0.468	0.447

marked as yellow, green, and blue. The burst pressure as per a particular failure criterion is the internal pressure load for which the average normal and shear stress components yield the failure parameter value of one as summarized in Table S1 of the supplementary information.

Similarly, finite element models have been reported in literature for predicting the bursting pressure of composite structures. Jadoon et al. has used reduced models to predict failure in inner two layers of the composite pressure vessel[43]. The first layer is reported to stay safe at 20 MPa working pressure while the second layer fails. However, the model proposed in this study can predict failure in all layers for every mesh element individually. Hereby, providing a detailed analysis of the safety of the cylinder during operation. Regassa et al. have also developed an FEA model to predict the effect of stacking sequence on burst pressure of a type-3 cylinder[44]. The thickness distribution of the composite layer has not been clearly discussed in the aforementioned literatures. The incorporation of thickness results in the FEA model aids in designing cylinders with lower weight without compromising with the burst safety of the cylinder.

3.2. Manufacturing the type-4 cylinder

The type-4 cylinder was wound using computer-controlled filament winding equipment, manufactured by CNC Technics, Hyderabad, India. It was a 6-axis filament winding machine equipped with a fiber delivery system, fiber tensioning/ spreading stations, resin impregnation unit, winding unit, and a controlling unit. The fiber delivery system consisted of a stand on which 6 fiber payoffs were mounted. Each payoff was fitted with a mechanical fiber tensioner for controlling the fiber tension. A dip-type resin drum impregnation system was used in which fibers were dipped in the resin bath for the impregnation. The configuration of the resin drum and the doctor blades affected the initial fiber band volume fraction at the payout eye. The excess resin was wiped off the fiber bands at the doctor blades, which were placed over the resin bath to collect back the wiped off resin during winding. The control system was programmed using CADFIL software developed by Crescent Consultants ltd, UK. It was used to determine the required fiber path for winding the type-4 cylinders for a given winding pattern. The type-4 composite cylinder was manufactured using the winding parameters given in Table 6. Six fiber spools were used simultaneously to wind the composite overwrap. The fiber volume fraction of the dissected composite overwrap is determined to be 0.4 ± 0.01 using loss on ignition test as per ASTM 2584-18.

3.3. Burst testing the vessel for validating the finite element model

A type-4 cylinder with a winding sequence as shown in Table 3, is manufactured using the manufacturing parameters of Table 6. The wound prototype is cured and valve fixtures are installed for burst

Table 10

Effect of different fibers on cost and performance of type-4 cylinders.

Fiber Type	No. of Layers	Burst Pressure (MPa)	Liner Weight (kg)	Composite Weight (kg)	Fiber weight (kg)	Resin Weight (kg)	Composite Cost (\$)
S Glass Fiber	44	74	5.69	42.8	26.75	16.05	193.3
E Glass Fiber	58	72	5.69	52.6	32.88	19.73	185.41
Kevlar-49 Aramid Fiber	44	76	5.69	43.2	27	16.2	1128.79
T700-12 K Carbon Fiber	27	70	5.69	25.2	15.75	9.45	1083.28

testing. The manufactured type-4 cylinder was tested for hydrostatic pressure burst test as per the international safety standard, ISO11439. The type-4 cylinder is filled with water and hung vertically in an underground pit. The pressure is increased at a rate of 0.35 MPa/s. The pressure at which the cylinder fails is known as the burst pressure of the type-4 cylinder. The burst pressure is found to be 77 MPa as shown in Figure S2 of the [supplementary information](#).

4. Results and discussion

Two models are developed in this study, an analytical model is developed to predict the composite thickness distribution and the layer-wise fibers consumption. An FEA model is developed to determine the burst pressure, failure characteristics, and weight of the manufactured type-4 cylinder; the details of the modeling plies are obtained from the analytical model. The results of the two models are used to design better-weight performing type-4 cylinders with required geometry and burst pressure. The raw material cost for the type-4 cylinder is also estimated using fiber consumption statistics. These models have been experimentally validated to check for their viability for predicting the aforementioned results.

4.1. Comparing theoretical and actual composite thickness distribution

The manufactured cylinder is dissected as shown in Fig. 7(A) to obtain the actual type-4 cylinder thickness distribution as shown in Fig. 7(B). The thickness at different locations on the type-4 cylinder is measured as shown in Fig. 7(C). The plastic liner is separated from the dissected portion to obtain the actual composite layer distribution as shown in Fig. 7(D). The obtained thickness distribution is measured as shown in Fig. 7(E-F). The actual results overlapped with the results of the developed analytical model to predict the composite thickness distribution as shown in Fig. 7(G). The results of the analytical model are given in Table 4 of Section 2.2. The predicted thickness of the type-4 composite vessel in the cylindrical section is 16.61 mm while the actual cylindrical thickness is obtained to be 15.72 mm. This is because hoop layers apply compaction pressure on previously wound layers dripping out the excess resin and reducing the thickness of the cylindrical section. The predicted thickness distribution in the dome section precisely overlaps with the actual results. This validates the model for predicting composite layer distribution for a given fiber bandwidth, initial fiber band volume fraction, winding sequence, and mandrel geometry.

The composite thickness distribution of the type-4 composite vessel predicted using this model is fed into the geometry details of the developed FEA model, to accurately predict the burst pressure and the failure characteristics of the type-4 cylinder.

4.2. Comparing the predicted layer-wise fiber consumption with the winding observations

The fiber weight consumed during the winding of individual composite layers is theoretically calculated using Equations (14) and (16). For the chosen liner geometry, two ellipses form in one cycle during 45° winding, ~1.5 ellipses are traversed during 35° winding, and ~1.25 ellipses are traversed in 25° winding. This value depends on the winding angle and the length of the cylindrical section of the mandrel. The theoretical values are compared with the experimental values obtained from the manufacturing information of the type-4 composite cylinder as given in Table 7.

The predicted fiber consumption is less than the actual usage, as the predicted model doesn't include the fiber path added for joining paths between one winding layer and another. The theoretical results lie within 5% error limits, hereby validating the analytical model for predicting the layer-wise amount of fiber consumed for winding a type-4 cylinder.

The resin consumption mainly depends on the configuration of the doctor blades, the resin viscosity, the winding speed, and the surface interactions between the fiber bands and the resin. The amount of resin used for manufacturing the type-4 cylinder can be determined experimentally for one set of material and machine parameters. For the given winding arrangement, the mass of resin used is ~ 0.689 times the weight of total fibers consumed. Therefore, the total consumption of the raw materials can be theoretically predicted using the developed analytical model. The model estimates the accurate amount of fiber consumed and gives an approximate value of resin consumption. The weight of the resin consumed cannot be estimated directly using the developed model as it depends on a variety of manufacturing parameters and surface interactions. The resin weight is theoretically predicted in Section 4.3 of this study. These results are used to estimate the raw material cost of the type-4 cylinder.

4.3. Validation of the FEA model

The failed regions of the tested type-4 cylinder were compared with the failure characteristics obtained using the ACP Pre-Post module as per different failure criteria. The failed cylinder is illustrated in Fig. S3(A) of the [supplementary information](#). The ruptured regions are identified and traced on a CAD drawing for comparison. The criterion which best overlaps with the actual failure is taken as the failure criterion for burst prediction. Hashin failure criterion is the criterion as per which, the elements marked with yellow contours have a failure parameter value of one and trace the path of rupture. The cracks don't enter the safest regions and pass through their boundaries. Therefore, the FEA model is validated for the Hashin failure criterion. The dimensional analysis of the failed regions as seen in the CAD drawing of Fig. S3(B) coincides with the Hashin failure characteristics for major cracks as illustrated in Fig. S3(C). The theoretical burst pressure value predicted as per the Hashin failure criterion is 75.3 MPa. The actual burst pressure is obtained to be 77 MPa which lies within the 5 % error range of acceptance. Therefore, the FEA model is validated for predicting the burst pressure and failure characteristics of a type-4 cylinder using experimental results.

The developed FEA model is also extended to estimate the weight of the type-4 cylinder theoretically. The weight of the plastic liner and composite overwrap defined in the FEA model as per the obtained composite thickness distribution is determined to be 5.69 kg and 29.59 kg respectively. The overall weight of the type-4 cylinder is theoretically determined to be 35.28 kg, while the weight of the manufactured type-4 cylinder is measured to be 35 kg.

The fiber weight can be discretely determined using the analytical model as validated in Section 4.2 of this study. The resin weight can be theoretically determined using the results of the FEA and the analytical model. The difference between the composite weight predicted by the FEA model (29.59 kg) and the fiber weight estimated from the analytical model (17.827 kg) gives the total resin weight i.e. 11.763 kg. Therefore, the models proposed in this study can be used to predict the composite thickness distribution, the fiber and resin consumption, the burst pressure, the failure characteristics, and the overall weight of the type-4 cylinder.

4.4. Statistical variations in composite thickness distribution

The composite thickness distribution of the type-4 vessel mainly depends on the initial fiber bandwidth, the initial fiber band volume fraction, the winding pattern, and the geometry of the mandrel. The validated models are used to optimize the composite thickness distribution to manufacture lighter type-4 cylinders with higher burst pressure.

4.4.1. Effects of initial bandwidth

The initial bandwidth as described in Equation (1), depends on the number of fiber spools, the percentage overlap between adjacent fibers

on the pay-out eye, and the bandwidth of each fiber band. These properties can be increased or decreased to vary the initial fiber bandwidth. The payout eye can be modified for increasing or decreasing the number of fiber spools that form a fiber band for winding. The partial overlaps between the fiber bands constituting the initial fiber bandwidth can also be increased or decreased by adjusting pulleys at the payout eye. The initial bandwidth of the fiber bands is varied from 9 to 30 mm by increasing the number of spools from one to six spools or by varying the bandwidth of individual fiber bands by partially overlapping them. The composite thickness distribution in different sections of the liner geometry for these bandwidths is calculated as per the previously validated model and summarized in [Table S2](#) and [Fig. 8\(A\)](#). The initial fiber band volume fraction is taken as 0.39. The calculations illustrate that the composite thickness distribution of the composite layers varies with the initial bandwidth.

4.4.2. Effects of band-thickness

For a given initial bandwidth, the thickness of the fiber bands at the payout eye varies with the initial fiber volume fraction in the fiber band during winding. The constant cross-sectional area of the wound fiber bands as defined in [Equation \(3\)](#), reduces with an increase in the fiber band volume fraction for a given number of fiber spools. The initial fiber band volume fraction is varied from 0.1 to 0.6. It is the possible range of fiber volume fraction variations for winding composites using the wet filament winding technique. For an initial bandwidth of 21 mm, the effects of fiber band volume fraction on the overall thickness distribution in different sections of the type-4 cylinder are summarized in [Fig. 8\(B\)](#) and [Table 8](#).

[Fig. 8](#) is the pictorial representation of the composite thickness as predicted in different sections of the cylinder. The dome section of the cylinder has been magnified and represented in the given figure and the composite thickness at different dome sections is predicted as per the developed analytical model for different values of initial bandwidth and initial fiber band volume fraction.

It is seen that the composite layer distribution significantly varies with the initial fiber band volume fraction. The fiber volume fraction also affects the mechanical properties of the composite following the micromechanics approach. The mechanical properties of the composite with given fiber volume fractions were calculated using the micromechanics approach and fed to the validated FEA model as the engineering data. The burst pressure and normalized composite weight of type-4 cylinders with composite thickness distributions calculated for the given fiber band volume fractions were determined as given in [Fig. 9\(A\)](#) and [\(B\)](#). Normalized weight is the weight of the composite that is required to add one MPa burst pressure to the total burst pressure value. The total weight for type-4 cylinders with a burst pressure of 72 MPa for given fiber band volume fractions is estimated from the normalized composite weights assuming the plastic liner weight to be 5 kg as given in [Fig. 9\(C\)](#).

4.4.3. Effect of winding sequence

Three different composite thickness distributions are obtained using different winding sequences, each with the same number of composite layers. The composite thickness in the cylindrical section is the same while that in the dome section differs as shown in [Figure S4](#) of the [supplementary information](#). The burst pressure and the weight of the type-4 vessel for each of the proposed composite thickness distributions are simulated using the validated FEA model. The burst pressure and the weight of vessels with these sequences are given in [Table 9](#). It is observed that for the same composite thickness in the cylindrical section, vessels designed to have composite thickness distribution 1 have a burst pressure of 79.86 MPa and the weight of the vessel is 38.97 kg. For type-4 cylinders with composite thickness distributions 2 and 3, the burst pressures are 80.5 MPa and 82.59 MPa, and the vessel weights are 37.69 kg and 38.92 kg respectively. The initial bandwidth and the initial fiber band volume fraction are taken to be 21 mm and 0.39 for these cases.

The weight of the vessel has been normalized to obtain the per kg weight of composite required to design type-4 cylinders with a given burst pressure. Therefore, the comparison illustrates that the burst pressure and weight of the type-4 cylinder are highly dependent on its composite thickness distribution.

4.5. Cost analysis

The cylinders were designed as per winding sequence 3 for better performance. The raw material cost was estimated using the results of the analytical and FEA model by estimating the fiber and resin consumption. Vessels with S glass, E glass, and Kevlar-49 fibers from Azo Materials, and T700 carbon fiber from Toray, Japan as reinforcement materials and epoxy resin as matrix system were designed for the required burst pressure of 70 MPa. The effects of using different fibers on the cost and performance of a type-4 pressure vessel were analyzed. The results of the cost analysis study are summarized in [Table 10](#), where the cost of S Glass, E Glass, Kevlar-49, and T700-12 K Carbon fibers are assumed to be \$4.66/kg, \$3.07/kg, \$39.23/kg, and \$66.2/kg respectively[[45,38](#)]. The cost of the resin hardener mixture is assumed to be \$3.98/kg. The initial fiber band volume fraction for all of these choices was assumed to be 0.39. The mechanical properties were calculated using the micromechanics approach.

5. Conclusion

An analytical model to determine the actual composite thickness distribution for any choice of reinforcement material, liner geometry, number of fiber spools, fiber bandwidth, winding pattern, and initial fiber band volume fraction is validated in this study. An FEA model to predict the burst pressure, failure characteristics, and weight of the type-4 cylinder is also developed and validated. The results illustrate that the initial fiber bandwidth, initial fiber band volume fraction, and the winding sequence play a significant role in affecting the performance of a type-4 composite vessel. Optimization of the initial fiber bandwidth improves the composite thickness distribution. The excess composite that bundles in the dome section can be reduced significantly by varying the initial bandwidth. The initial fiber band volume fraction improves the composite thickness distribution and also affects the load-bearing characteristics of the composite, yielding cylinders with high burst pressure and reduced weights. The burst and weight performance of the type-4 cylinders are also affected by their winding sequences. The proposed composite thickness distributions (1, 2, and 3) had the same composite thickness in the cylindrical section, however, their burst pressures were 79.86 MPa, 80.5 MPa, and 82.59 MPa respectively. Therefore, the composite thickness distribution can be varied based on the product requirements and manufacturing feasibility using the developed models. The models for optimizing the composite thickness distribution, determining the fiber and resin consumption, and predicting the burst pressure and weight of the type-4 cylinder are established, thereby improving the product performance without compromising its storage safety. It also helps to design low-cost type-4 cylinders by choosing appropriate reinforcement materials based on the weight requirements and the application.

Data Availability Statement

The raw/processed data required to reproduce these findings cannot be shared at this time due to legal or ethical reasons.

CRediT authorship contribution statement

Pranjali Sharma: Conceptualization, Methodology, Software. **Swati Neogi:** Conceptualization, Methodology, Writing – review & editing.

Declaration of Competing Interest

The authors declare that they have no known competing financial

interests or personal relationships that could have appeared to influence the work reported in this paper.

Data availability

The data that has been used is confidential.

Acknowledgement

None.

Appendix A. Supplementary data

Supplementary data to this article can be found online at <https://doi.org/10.1016/j.compstruct.2023.116710>.

References

- [1] Sorrentino L, Anamateros E, Bellini C, Carrino L, Corcione G, Leone A, et al. Robotic filament winding: An innovative technology to manufacture complex shape structural parts. *Compos Struct* 2019;220:699–707. <https://doi.org/10.1016/j.compstruct.2019.04.055>.
- [2] Fu J, Yun J, Jung Y, Lee D. Generation of filament-winding paths for complex axisymmetric shapes based on the principal stress field. *Compos Struct* 2017;161: 330–9. <https://doi.org/10.1016/j.compstruct.2016.11.022>.
- [3] Sharma P, Sardar HH, Neogi S. Thermomechanical processing of Type-4 composite cylinders under static load. *J Energy Storage* 2022;55:105465. <https://doi.org/10.1016/j.est.2022.105465>.
- [4] Quanjin M, Rejab MRM, Kaige J, Idris MS, Harith MN. Filament winding technique, experiment and simulation analysis on tubular structure. IOP Conf Ser Mater Sci Eng 2018;342:12029. <https://doi.org/10.1088/1757-899x/342/1/012029>.
- [5] Shen K-C, Pan G. Buckling and strain response of filament winding composite cylindrical shell subjected to hydrostatic pressure: Numerical solution and experiment. *Compos Struct* 2021;276:114534. <https://doi.org/10.1016/j.compstruct.2021.114534>.
- [6] Eycckens DJ, Stojcevski F, Hendlmeier A, Arnold CL, Randall JD, Perus MD, et al. An efficient high-throughput grafting procedure for enhancing carbon fiber-to-matrix interactions in composites. *Chem Eng J* 2018;353:373–80. <https://doi.org/10.1016/j.cej.2018.07.133>.
- [7] Sharma P, Sharma S, Bera T, Semwal K, Badhe RM, Sharma A, et al. Effects of dome shape on burst and weight performance of a type-3 composite pressure vessel for storage of compressed hydrogen. *Compos Struct* 2022;293:115732. <https://doi.org/10.1016/j.compstruct.2022.115732>.
- [8] Panchagnula KK, Panchagnula JS. Fabrication of hoop-wound glass fiber reinforced plastic cylindrical shells using filament winding machine. *Mater Today Proc* 2020; 27:1315–8. <https://doi.org/10.1016/j.mtpr.2020.02.349>.
- [9] Zhang X, Zhao J, Wang Z. Burst Pressure Prediction and Structure Reliability Analysis of Composite Overwrapped Cylinder. *Appl Compos Mater* 2018;25: 1269–85. <https://doi.org/10.1007/s10443-017-9665-x>.
- [10] Dahl E, Becker JS, Mittelstedt C, Schürmann H. A new concept for a modular composite pressure vessel design. *Compos Part A Appl Sci Manuf* 2019;124: 105475. <https://doi.org/10.1016/j.compositesa.2019.105475>.
- [11] Li C, Yao T, He X, Zhou C. Stress analysis for the orthotropic pressurized structure of the cylindrical shell and spherical head. *Thin-Walled Struct* 2017;111:29–37. <https://doi.org/10.1016/j.tws.2016.11.003>.
- [12] Jeong HD, Kim SG, Choi GM, Park M, Ku B-C, Lee HS. Theoretical and experimental investigation of the wet-spinning process for mechanically strong carbon nanotube fibers. *Chem Eng J* 2021;412:128650. <https://doi.org/10.1016/j.cej.2021.128650>.
- [13] Jia X, Chen G, Yu Y, Li G, Zhu J, Luo X, et al. Effect of geometric factor, winding angle and pre-crack angle on quasi-static crushing behavior of filament wound CFRP cylinder. *Compos Part B Eng* 2013;45:1336–43. <https://doi.org/10.1016/j.compositesb.2012.09.060>.
- [14] Shen KC, Pan G, Lu J. Buckling and layer failure of composite laminated cylinders subjected to hydrostatic pressure. *Sci Eng Compos Mater* 2017;24:415–22. <https://doi.org/10.1515/secm-2015-0172>.
- [15] Sharma P, Bera T, Semwal K, Badhe RM, Sharma A, Ramakumar SSV, et al. Theoretical analysis of design of filament wound type 3 composite cylinder for the storage of compressed hydrogen gas. *Int J Hydrogen Energy* 2020;45:25386–97. <https://doi.org/10.1016/j.ijhydene.2020.06.269>.
- [16] Roh HS, Hua TQ, Ahluwalia RK. Optimization of carbon fiber usage in Type 4 hydrogen storage tanks for fuel cell automobiles. *Int J Hydrogen Energy* 2013;38: 12795–802. <https://doi.org/10.1016/j.ijhydene.2013.07.016>.
- [17] Shen K, Pan G, Jiang J. Design optimization of composite cylinders for submersible pressure hulls 2016. <https://doi.org/10.2991/mmse-16.2016.120>.
- [18] Vafaeesefat A, Khani A. Head Shape and Winding Angle Optimization of Composite Pressure Vessels Based on a Multi-level Strategy. *Appl Compos Mater* 2007;14: 379–91. <https://doi.org/10.1007/s10443-008-9052-8>.
- [19] Geng P, Xing J, Wang Q. Analytical model for stress and deformation of multiple-winding-angle filament-wound composite pipes/vessels under multiple combined loads. *Appl Math Model* 2021;94:576–96. <https://doi.org/10.1016/j.apm.2021.01.034>.
- [20] Zu L, Xu H, Wang H, Zhang B, Zi B. Design and analysis of filament-wound composite pressure vessels based on non-geodesic winding. *Compos Struct* 2019; 207:41–52. <https://doi.org/10.1016/j.compstruct.2018.09.007>.
- [21] H. Li, Y. Ma, Filament winding pattern design for diameter-varying tube, (2022). Doi: 10.1177/07316844221135174.
- [22] G. Park, H. Jang, C. Kim, Design of composite layer and liner for structure safety of hydrogen pressure vessel (type 4), 35 (2021). Doi: 10.1007/s12206-021-04.
- [23] Mazurkiewicz Ł, Małachowski J, Damaział K, Tomaszewski M. Evaluation of the response of fibre reinforced composite repair of steel pipeline subjected to puncture from excavator tooth. *Compos Struct* 2018;202:1126–35. <https://doi.org/10.1016/j.compstruct.2018.05.065>.
- [24] Adak NC, Sharma P, Sardar HH, Neogi S. Model Verification and Determination of Temperature-Dependent Mechanical Deformations of Short Glass Fiber / Vinyl Ester Composite by Using Laser Extensometer. *J Mater Eng Perform* 2022. <https://doi.org/10.1007/s11665-022-07528-3>.
- [25] Hernández-Moreno H, Douchin B, Collombet F, Choqueuse D, Davies P. Influence of winding pattern on the mechanical behavior of filament wound composite cylinders under external pressure. *Compos Sci Technol* 2008;68:1015–24. <https://doi.org/10.1016/j.compscitech.2007.07.020>.
- [26] Calius EP, Springer GS. A model of filament-wound thin cylinders. *Int J Solids Struct* 1990;26:271–97. [https://doi.org/10.1016/0020-7683\(90\)90041-S](https://doi.org/10.1016/0020-7683(90)90041-S).
- [27] Sharma P, Chugh P, Neogi S. Study to methodize the design of a safe Type-4 CNG storage vessel using finite element analysis with experimental validation. *Int J Press Vessel Pip* 2021;192:104425. <https://doi.org/10.1016/j.ijpvp.2021.104425>.
- [28] Molavizadeh A, Rezaei A. Progressive Damage Analysis and Optimization of Winding Angle and Geometry for a Composite Pressure Hull Wound Using Geodesic and Planar Patterns. *Appl Compos Mater* 2019;26:1021–40. <https://doi.org/10.1007/s10443-019-09764-8>.
- [29] Maleki S, Tahani M. Composites : Part B Non-linear analysis of fiber-reinforced open conical shell panels considering variation of thickness and fiber orientation under thermo-mechanical loadings. *Compos Part B* 2013;52:245–61. <https://doi.org/10.1016/j.compositesb.2013.04.026>.
- [30] J. Fu, J. Yun, J. Jung, Winding Trajectory Generation for Composite Products, 542 (2014) 407–411. Doi: 10.4028/www.scientific.net/AMM.541-542.407.
- [31] Lossie M, Van Brussel H. Design principles in filament winding. *Compos Manuf* 1994;5:5–13. [https://doi.org/10.1016/0956-7143\(94\)90014-0](https://doi.org/10.1016/0956-7143(94)90014-0).
- [32] Magnucki K, Jasion P, Rodak M. Strength and buckling of an untypical dished head of a cylindrical pressure vessel. *Int J Press Vessel Pip* 2018;161:17–21. <https://doi.org/10.1016/j.ijpvp.2018.02.003>.
- [33] Li M, Fan H. Multi-failure analysis of composite Isogrid stiffened cylinders. *Compos Part A Appl Sci Manuf* 2018;107:248–59. <https://doi.org/10.1016/j.compositesa.2018.01.010>.
- [34] Kobayashi S, Kawahara M. Effects of stacking thickness on the damage behavior in CFRP composite cylinders subjected to out-of-plane loading. *Compos Part A Appl Sci Manuf* 2012;43:231–7. <https://doi.org/10.1016/j.compositesa.2011.10.004>.
- [35] Liu PF, Chu JK, Hou SJ, Xu P, Zheng JY. Numerical simulation and optimal design for composite high-pressure hydrogen storage vessel: A review. *Renew Sustain Energy Rev* 2012;16:1817–27. <https://doi.org/10.1016/j.rser.2012.01.006>.
- [36] Leh D, Magneville B, Saffré P, Francescato P, Arrieux R, Villalonga S. Optimisation of 700 bar type IV hydrogen pressure vessel considering composite damage and dome multi-sequencing. *Int J Hydrogen Energy* 2015;40:13215–30. <https://doi.org/10.1016/j.ijhydene.2015.06.156>.
- [37] Colombo C, Vergani L. Optimization of filament winding parameters for the design of a composite pipe. *Compos Part B Eng* 2018;148:207–16. <https://doi.org/10.1016/j.compositesb.2018.04.056>.
- [38] Rafiee R, Habibagahi MR. Evaluating mechanical performance of GFRP pipes subjected to transverse loading. *Thin-Walled Struct* 2018;131:347–59. <https://doi.org/10.1016/j.tws.2018.06.037>.
- [39] Parashar A, Mertiny P. Failure mechanism in adhesively bonded FRP pipe sections with different fibre architecture. *Compos Part B Eng* 2013;47:102–6. <https://doi.org/10.1016/j.compositesb.2012.10.041>.
- [40] Tang Z, Wang C, Yu Y. Failure response of fiber-epoxy unidirectional laminate under transverse tensile/compressive loading using finite-volume micromechanics. *Compos Part B Eng* 2015;79:331–41. <https://doi.org/10.1016/j.compositesb.2015.04.054>.
- [41] Quanjin M, Rejab MRM, Idris MS, Bachtiar B, Siregar JP, Harith MN. Design and optimize of 3-axis filament winding machine. IOP Conf Ser Mater Sci Eng 2017; 257. <https://doi.org/10.1088/1757-899X/257/1/012039>.
- [42] Springer G, Wang SS. Failure of composite materials. *Appl Mech Rev* 1990;43: S280. <https://doi.org/10.1115/1.3120828>.
- [43] A. De Elementos, P. Compuestos, M. Modelos, M. Muzamil, Finite Element Analysis of Composite Pressure Vessel Using Reduced Models, 17 (2022) 49–62.
- [44] Regassa BSY, Lemu HG. Burst strength analysis of composite overwrapped pressure vessel using finite element method. *Burst strength analysis of composite overwrapped pressure vessel using finite element method*. IOP Conf Ser Mater Sci Eng 2021;1201. <https://doi.org/10.1088/1757-899X/1201/1/012029>.
- [45] Alibaba.com, accessed 22 November 2022, <<https://www.alibaba.com/trade>>.